ELSEVIER

Thermochimica Acta 362 (2000) 145–151

thermochimica acta

www.elsevier.com/locate/tca

Oxidation of marmatite☆

R.I. Dimitrov[a,*], N. Moldovanska[b], I.K. Bonev[c], Ž Živkovic[d]

[a]*Department of Fundamentals of Chemical Technology, University of Chemical Technology and Metallurgy, 8 Kliment Ohridski Blvd., 1756 Sofia, Bulgaria*

[b]*Department of Inorganic Chemical Technology, University of Plovdiv, 24 Tsar Assen Street, 4000 Plovdiv, Bulgaria*

[c]*Geological Institute, Bulgarian Academy of Science, 1113 Sofia, Bulgaria*

[d]*Technical Faculty at Bor, 19210 Bor, Yugoslavia*

Received 1 October 1999; received in revised form 18 April 2000; accepted 27 June 2000

Abstract

As a continuation of our long-term investigation of the thermodynamics, kinetics and mechanism of metal sulphide oxidation the present paper present results on the Marmatite oxidation, using DTA, TGA, X-ray diffraction analysis, optical and scanning electron microscopy (SEM).

The paper presents three-dimensional diagrams of partial pressures of SO_2 and O_2 against T for the Zn-Fe-S-O system.

A multi-layer oxide product of high porosity (over 30%) was obtained as shown by scanning electron microscopy. On the basis of kinetic studies and electron microscopy, it was found that under the conditions of zinc concentrates fluid bed roasting, the oxidation of marmatite takes place in a kinetically controlled regime.

Keywords: Marmatite; Oxidation; Thermodynamic; Kinetics; Mechanism; DTA; TGA; SEM

1. Introduction

The form of zinc and iron sulphides in zinc concentrates is of importance for its pyrometallurgical processing. Presence of marmatite results in a considerable increase in the formation of zinc ferrite [1–3] which is insoluble in diluted solutions of sulphuric acid.

In previous research [4–6] experiments have been made with synthetic amorphous and crystal ZnS and a natural mineral-sphalerite.

The purpose of the present study is to investigate oxidation of rich of Fe sphalerite [marmatite — (Zn, Fe)S] in air under isothermal conditions (roasting in furnace) and non-isothermal (DTA-TG) conditions.

2. Experimental

Chemical analysis of marmatite gave following chemical composition: 54.2% Zn; 10.8% Fe; 33.6% S; 1.4% others.

Differential thermal and thermogravimetric analyses were carried out using a Q Derivatograph, manufactured by MOM, Hungary. The analyses were made in air within a platinum crucible using the following sensitivities: DTA 0.5 mV; DTG 1 mV; TG 100 mg. The mass of the sample was 100 mg at a heating rate of 10 K min^{-1}. The particles size was

☆Part of results has been reported at 36th IUPAC Congress, Geneva, Switzerland, 17–22 August 1997.

* Corresponding author. Tel.: +359-2-6254-485; fax: +359-2-6254-485.

E-mail address: rumen@uctm.edu (R.I. Dimitrov).

0040-6031/00/$ – see front matter
PII: S0040-6031(00)00582-7

under 0.1 mm. Al_2O_3 was used as the reference material.

The calcine produced was analysed by X-ray diffraction using a TUR-M61 diffractometer (Germany), with a Co tube and an Fe filter.

Oxidised products were examined as broken fragments and as polished sections by optical microscopy, SEM and SEI.

3. Results and discussion

3.1. DTA-analyses

Fig. 1 presents DTA-TG-DTG-responses of marmatite oxidation with temperature up to 1000°C.

The weak exotherm at about 460°C is due to the dissociation of small quantities of pyrite present. The initial increase in sample mass was a result of partial sulphatisation of FeS present in marmatite. The broad intense exotherm in the interval 600–800°C was due to the formation of $FeSO_4$, which subsequently dissociated and sulphatisation of ZnS to $ZnSO_4$. This interpretation is based on the analysis of the DTG which displayed the presence of several processes which merge in the DTA response. The endotherms are due to the two-stage dissociation of $ZnSO_4$, i.e. $ZnSO_4 \rightarrow ZnO \cdot 2ZnSO_4 \rightarrow ZnO$.

3.2. Thermodynamic analysis

A number of authors [7–11] have recommended that the stable phases in the system should be assigned on the basis of partial pressure diagrams of the gas components.

A three-dimensional diagram of the Zn-Fe-S-O system in the temperature interval 750–1000°C with coordinates — $\log P_{SO_2} - \log P_{O_2} - T$ is shown in Fig. 2. Stable phases at partial pressures of the gas components within the following limits: O_2

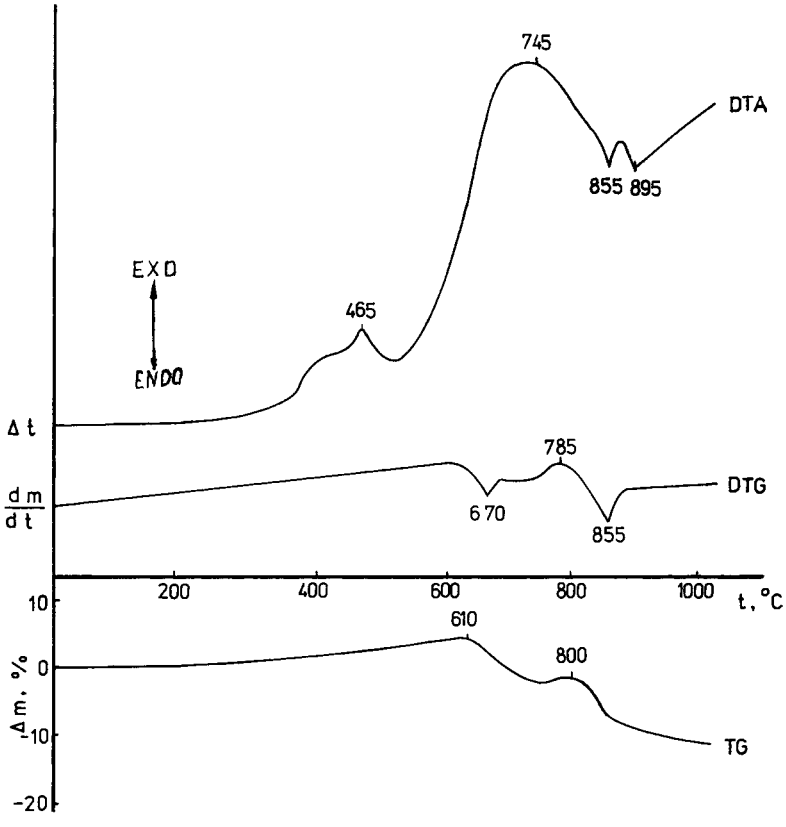

Fig. 1. DTA-TG-DTG diagrams of marmatite.

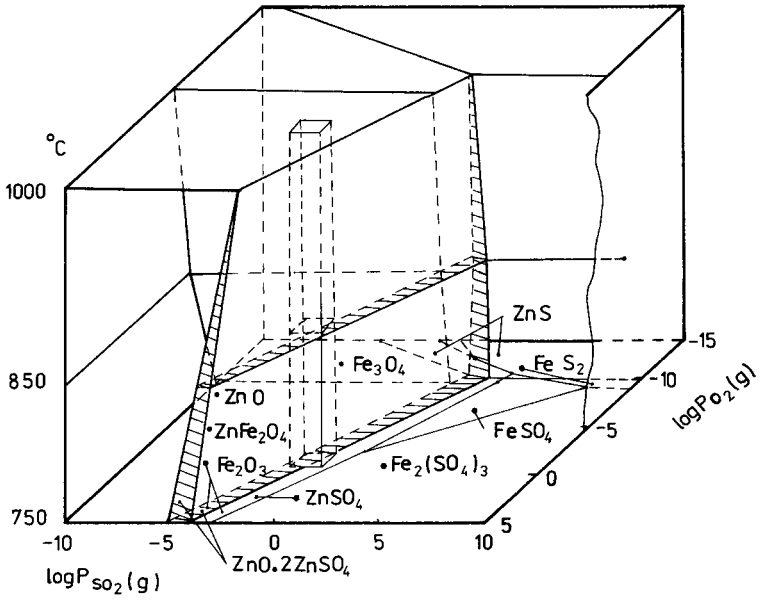

Fig. 2. Three-dimensional diagrams of partial pressures of the Zn-Fe-S-O system in coordinates $\log P_{SO_2} - \log P_{O_2} - T$.

content from 1 to 21% and SO_2 from 1 to 14% were determined.

The thermodynamically stable phases in the Zn-Fe-S-O system are

$750^{\circ}C \rightarrow Fe_2O_3\text{-}ZnO\text{-}ZnO \cdot 2ZnSO_4\text{-}ZnFe_2O_4\text{-}(ZnSO_4)^*$

$850^{\circ}C \rightarrow Fe_2O_3\text{-}ZnO\text{-}ZnFe_2O_4\text{-}(ZnO \cdot 2ZnSO_4)^*$

$1000^{\circ}C \rightarrow Fe_2O_3\text{-}ZnO\text{-}ZnFe_2O_4$

*( ) — phase, stable only at certain temperature and gas phase composition.

From a thermodynamic point of view and at the temperature interval studied the following phases were the most stable: ZnO, Fe_2O_3 and $ZnFe_2O_4$. $ZnSO_4$ and $ZnO \cdot 2ZnSO_4$.are stable only at comparatively low temperatures ($ZnSO_4$ up to about 850°C and $ZnO \cdot 2ZnSO_4$up to about 950°C.)

The diagram shown in Fig. 2 is made using the method described in [11,12].

3.3. Kinetic analysis of a marmatite crystal roasting under isothermal conditions

The oxidation was carried out in a roasting furnace under laboratory conditions. The mass of crystalline samples was 200 mg. The oxidant was air. The extent of desulphurisation of marmatite was followed at each temperature: 750, 850, 950 and 1000°C.

The results obtained for the extent of reaction $\alpha = f(t)$ at constant temperature and heating time of 1 h are shown in Fig. 3.

The kinetics were analysed using the method of Levenspiel [13] and Habashi [14] for the $S_1 + G_1 = S_2 + G_2$ system on the basis of the following

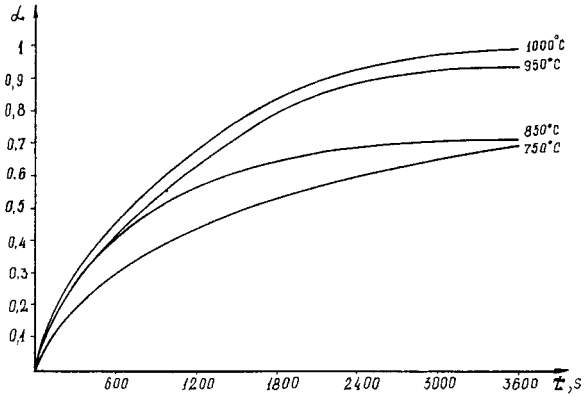

Fig. 3. Changes in the degree of desulphurization with time at roasting temperatures of: (a) 750; (b) 850; (c) 950; (d) 1000°C.

equations:

(a) $F(\alpha) = 1 - (1-\alpha)^{1/3} = Kt$

This equation of Levenspiel and Habashi is for the formation of a porous product, when the limiting stage of the heterogeneous process is the chemical reaction at the interface of reagent and product.

(b) $1 - \frac{2}{3}\alpha - (1-\alpha)^{2/3} = Kt$

The equation of Crank, Ginstling and Braunstein is for the formation of a nonporous product, where the gaseous reagent diffuses through the solid product towards the unreacted cores and diffusion is the rate-limiting stage.

Analysis of the extent of reaction against time showed that only the first equation was applicable.

The apparent activation energy of the process for the temperature interval 750–1000°C was determined from the Arhenius equation: $\ln K = \ln K_0 - (E_a/RT)$ and gave a value of 80 kJ mol^{-1} which is in good agreement with the values 69 kJ mol^{-1} determined by the Kissinger method and 86 kJ/mol by the Ozawa method [10].

According to [15], reactions with $E_a > 41$ kJ mol^{-1} take place in a kinetic regime. Our investigations show that the process of marmatite oxidation takes place with rate limiting step being the chemical reaction, and not the resistance of the newly formed product.

3.4. X-ray analysis of the obtained calcine

The X-ray diagrams of the initial marmatite sample and the calcine, obtained at temperatures 750, 850 and 1000°C are shown in Fig. 4.

The thermodynamically stable phases ($ZnSO_4$ at 750°C and $ZnO \cdot 2ZnSO_4$at 850°C) were not present in the calcine and no Fe_2O_3 was determined. It is suggested that all the iron is in the form of $ZnFe_2O_4$.

3.5. Scanning electron microscope study

To study the complicated oxidation process an, iron-rich, dark-brown, large crystals of sphalerite (marmatite) obtained from skarn lead–zinc deposit *Trepcha* in Kossovo, Jugoslavia, was used. The sphalerite composition according to microprobe analysis (averaged 3 samples) was: 33.58 S; 10.98 Fe; 1.30 Mn; 54.07 Zn; 0.14 Cd, a total of 100.07 wt.% and was of nearly homogeneous distribution. Its formula is $(Zn_{0.79}Fe_{0.19}Mn_{0.02})S_1$. No chalcopyrite or other solid inclusions (''chalcopyrite disease'') were established in sphalerite under reflection microscopy, and no Cu content detected. Only rare, very thin pyrite veinlets crosscut the crystal.

Homogeneously cleaved (along {1 1 0} planes) fragments of the sphalerite crystals were heated in a furnace at 850 and 1000°C for 60 min, with control of the *T*, weight, and the released gas of SO_2. The degree of desulphurization was about 40 and 59 wt.%, respectively.

X-ray powder diffraction study of the oxide product showed the presence ot two newly formed phases: ZnO, zincite, and $ZnFe_2O_4$, franklinite, a ferrite with a spinel structure. The microprobe analyses showed the nearly stoichiometric compositions of the oxide phases though precise franklinite analysis was not possible due to its small size. All the Mn was included in franklinite. It has been shown by Lucchesi et al. [16] that Mn, up to 10–12.9 wt.% MnO in natural franklinites, together with Zn occupies the tetrahedral sites in the normal spinel structure of this mineral, thus preserving the ratio $(Zn + Mn)/Fe = 1/2$.

Broken cross sections of the oxidised fragments were examined under scanning electron microscope (SEM) after carbon and gold coating. As can be seen in Fig. 5a and b, the unchanged central sulphide core is preserved surrounded by peripheral multi-layer oxide zone of high porosity and specific structure. This zone consists of numerous very fine layers of thickness up to 10 μm almost parallel to the particle surface. The single layers have a spongy texture and are composed of very fine submicron sized isometric oxide grains with similar pores between them.

The inhomogeneous structure of these layers is clearly seen in polished cross sections by optical microscopy and especially well in the back-scattered electron (BSE) images in the microprobe (Fig. 5c and d). It consist of darker ferrite and white zincite grains the size of which is smaller than 1 μm.

The area analysis shows that the initial average (Zn + Mn)/Fe metal ratio of ∼4:1 in the product is approximately preserved. Sometimes it is a bit lower due to restricted sublimation processes. Franklinite occupies the central part of the fine oxide layers being bilaterally overgrown by zincite crystals.

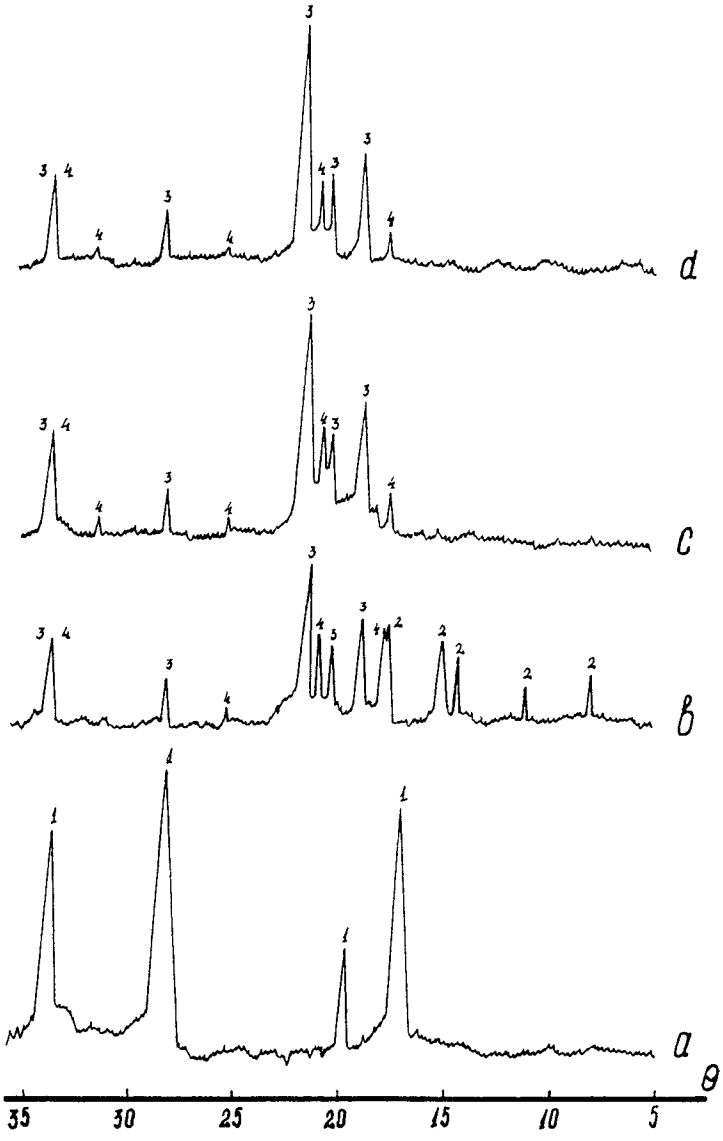

Fig. 4. X-ray diagrams of marmatite: (a) initial sample; (b) marmatite oxidized at 750°C; (c) marmatite oxidized at 850°C; (d) marmatite oxidized at 1000°C. Also (1) nZnS·mFeS; (2) ZnO · 2ZnSO$_4$; (3) ZnO; (4) ZnO·Fe$_2$O$_3$.

The high porosity (over 30%) of the replacing oxidation products is due to their smaller molecular volume in relation to the initial sulphide volume.

Sphalerite oxidation is an topochemical reconstructive process mostly preserving the initial location of the metal cations. The significant volume reduction is expressed by the high porosity of the fine-grained product, revealed: (1) as concentric cracks between the fine oscillating oxide layers, and (2) as uniform intergranular pores inside the layers. The replacement is of strongly pseudomorphic character, reproducing the original shape of particles and all fine details of their surface structure, like steps, cleavage planes, striations, twinning areas, and even fluid inclusion vacuoles. At higher T (>1000°C) some transport of ZnO can be realised also by sublimation at short distances, followed by condensation in some larger open pits.

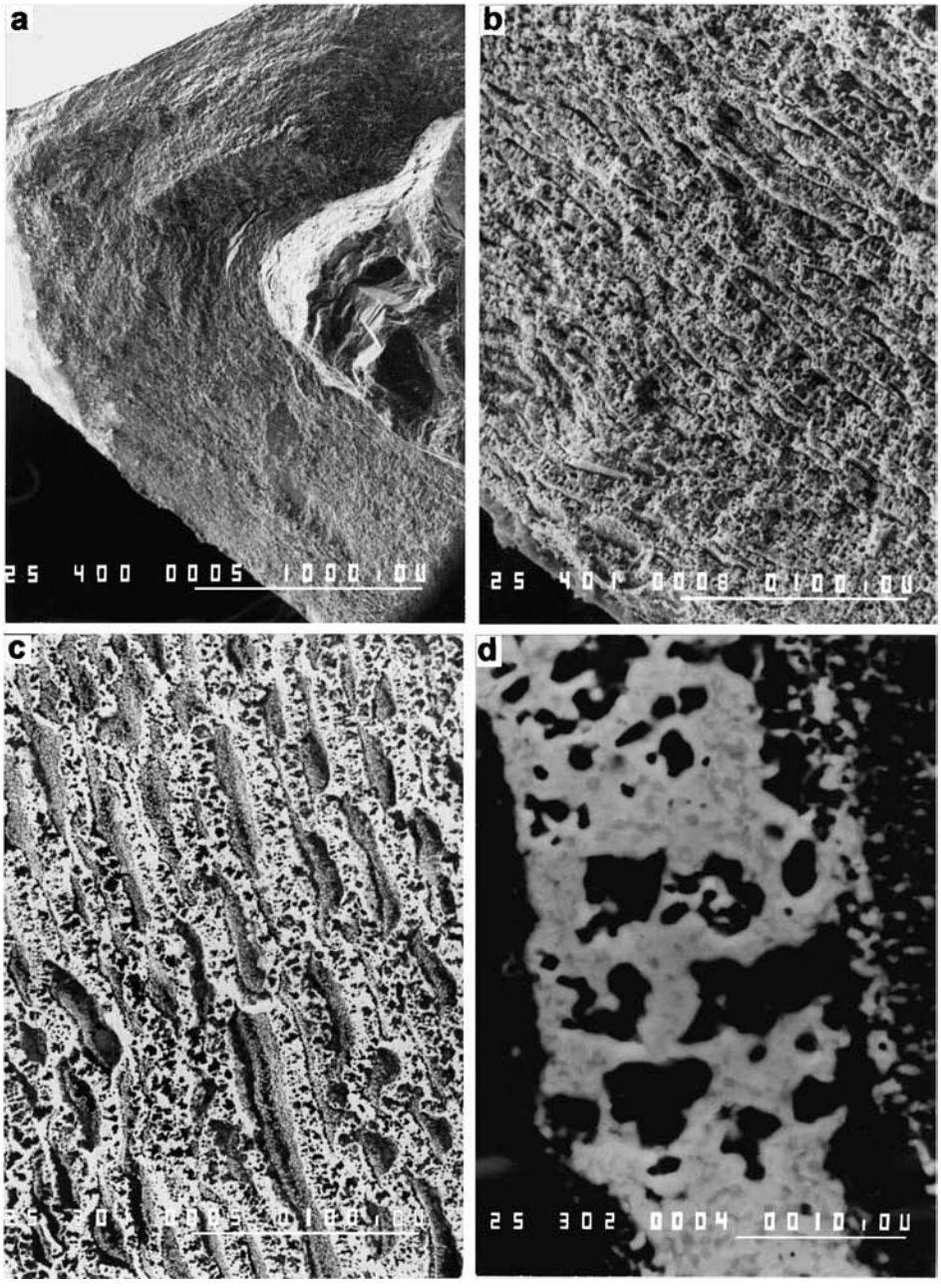

Fig. 5. Fine-layered spongy structure of the oxide crust replacing a high-iron sphalerite particle (partly preserved — on the right side) during the thermal oxidation at 1000°C: (a) general view, SEM; (b)detail; (c) rhythmic structure of the crust, back-scattered image (BSE); (d) enlarged BSE image showing the phase relationships: white — ZnO, gray — zinc-ferrite, black — pores.

The highly porous structure of the oxidised zone ensures uninterrupted diffusion supply of fresh air towards the reacting central sulphide core and back current of the newly produced SO_2 gas. Thus, the porous oxide mass is not a hindrance for the development of an oxidising process under a kinetic regime. Therefore, in general, mechanisms of this process for iron-free and iron-rich sphalerites are very similar.

4. Conclusion

The thermodynamic analysis carried out, and the three-dimensional phase diagram of partial pressures for the Zn-Fe-S-O system show the variation of stability of the different phases of calcine in a fluid bed roasting of marmatite against temperature and composition of the gas phase (content of O_2: 1–21% and of SO_2: 1–14%).

From a thermodynamic point of view, the following phases are stable at temperatures lower than 850°C: ZnO, $ZnO \cdot 2ZnSO_4$, $ZnSO_4$, Fe_2O_3 and $ZnFe_2O_4$. At temperatures exceeding 850°C and under the industrial conditions of roasting (900–1000°C and fluid bed) the following phases are stable: ZnO, Fe_2O_3 and $ZnFe_2O_4$.

Electron microscopy analysis shows the presence of multi-layer oxide product of high porosity (over 30%). X-ray diffraction analysis, as well as electron microscopy detect no presence of Fe_2O_3 in the product of roasting. All the Fe content of marmatite in the process of its oxidation combines into $ZnFe_2O_4$. This impedes the hydrometallurgical processing of zinc concentrates rich in marmatite, and necessitates the search for relevant methods for solving this problem.

Kinetic rate studies gave a value for E_a of about 80 kJ mol^{-1}. When zinc concentrates are roasted under industrial conditions (fluid bed, temperature of 900–1000°C, small-sized particles), marmatite is oxidised in a kinetically controlled regime. In this aspect the mechanism of oxidation of sphalerite containing a minimal quantity of Fe [4] and that of oxidation of sphalerite with higher content of Fe (marmatite) were quite similar.

References

[1] R. Dimitrov, P. Bakardziev, Mining Metall. Quart. (Ljubljana) 3/4 (1965) 347.
[2] R. Dimitrov, B. Boyanov, Mining Metall. Quart. (Ljubljana) 2/3 (1983) 211.
[3] B. Boyanov, R. Dimitrov, Thermochim. Acta 296 (1997) 123.
[4] R. Dimitrov, I. Bonev, Thermochim. Acta 106 (1986) 9.
[5] D. Schultze, U. Steinike, J. Kussin, U. Kretzschemer, Cryst. Res. Technol. 30 (4) (1995) 553.
[6] M. Galant Francois, F. Patisson, D. Ablitur, in: Proceedings of the 51st Congress of Annual Association of Brass Metallurgical Materials, Vol. 4, 1996, p. 57
[7] R. Benner, H. Kenworthy, RI bureau of mines, US Department, 1966, p. 1.
[8] A. Yazawa, Metall. Trans. B 10 (B) (1979) 307.
[9] J. Kruger, R. Pullenberg, Erzmetall 33, Germany 2 (1980) 70.
[10] Ž. Živković, D. Živković, D. Grujicić, V. Savović, Thermochim. Acta 315 (1998) 33.
[11] A. Pashinkin, M. Spivak, A. Malkova, Using Diagrams of Partial Pressures in Metallurgy, Metalurgia, Moscow, 1984 (in Russian).
[12] R. Dimitrov, N. Moldovanska, V. Stefanova, Rudarsko-Metall. Zb. (Ljubliana) 44 (3/4) (1997) 249.
[13] C. Levenspiel, Chemical Reaction Engineering, Wiley, New York, 1962.
[14] F. Habashi, Chemiker-Zeitung (Chem. Apparatur) Verfahrenstechnik (1969) 93.
[15] F. Habashi, Principles of extractive metallurgy, General Principles, Vol.1, Gordon and Breach, New York, 1972, p. 66.
[16] S. Lucchesi, U. Russo, A. Della Giusta, Eur. J. Mineral 11 (3) (1999) 501.